Supplement of Atmos. Chem. Phys., 23, 14801–14812, 2023
https://doi.org/10.5194/acp-23-14801-2023-supplement

Atmospheric Chemistry and Physics
Open Access

Supplement of

Seasonal variations in composition and sources of atmospheric ultrafine particles in urban Beijing based on near-continuous measurements

Xiaoxiao Li et al.

Correspondence to: James N. Smith (jimsmith@uci.edu) and Jingkun Jiang (jiangjk@tsinghua.edu.cn)

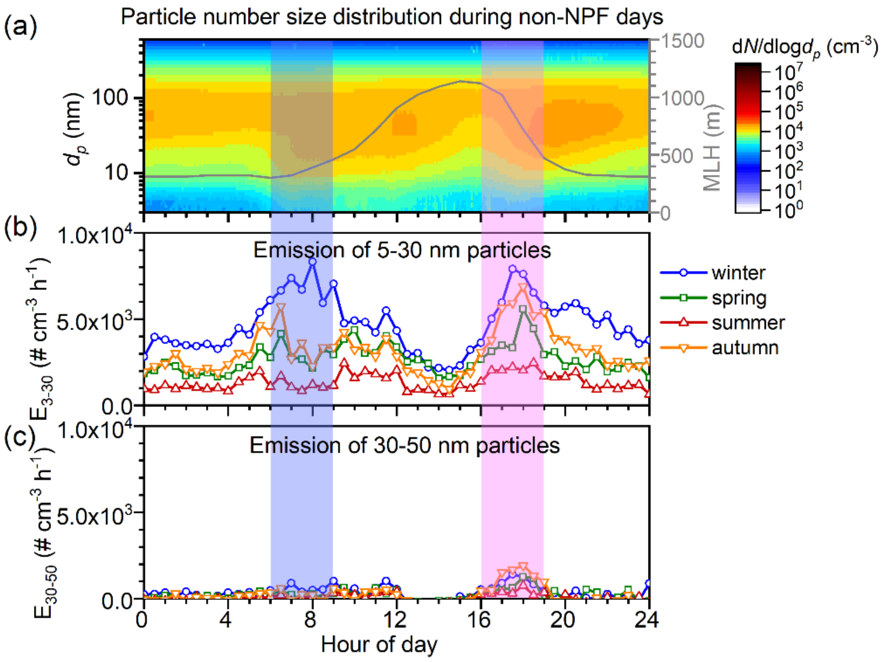

Figure S1. (a) Average diurnal variations of the particle size distributions during all the non-NPF days. The calculated emission rates for (b) 3-30 nm particles and (c) 30-50 nm particles. The number concentration valley at ~16:00 is possibly caused by the highest MLH, which increases from 8:00 in the morning to the highest in 16:00, then gradually decreases to the lowest until ~18:00. The number concentration peak at ~8:00 is possibly introduced by the emissions of 3-30 nm particles because that the emission of 30-50 nm particles does not increase simultaneously with 3-30 nm particles. The number concentration peak at ~18:00 is accompanied by both the emission of 3-30 nm particles and the 30-50 nm particles, they could be caused by a combined effect of the decrease of MLH, as well as primary emissions, or transportation. As a result, the morning peak at ~8:00 is chosen to study the primary emission rates in the main text.

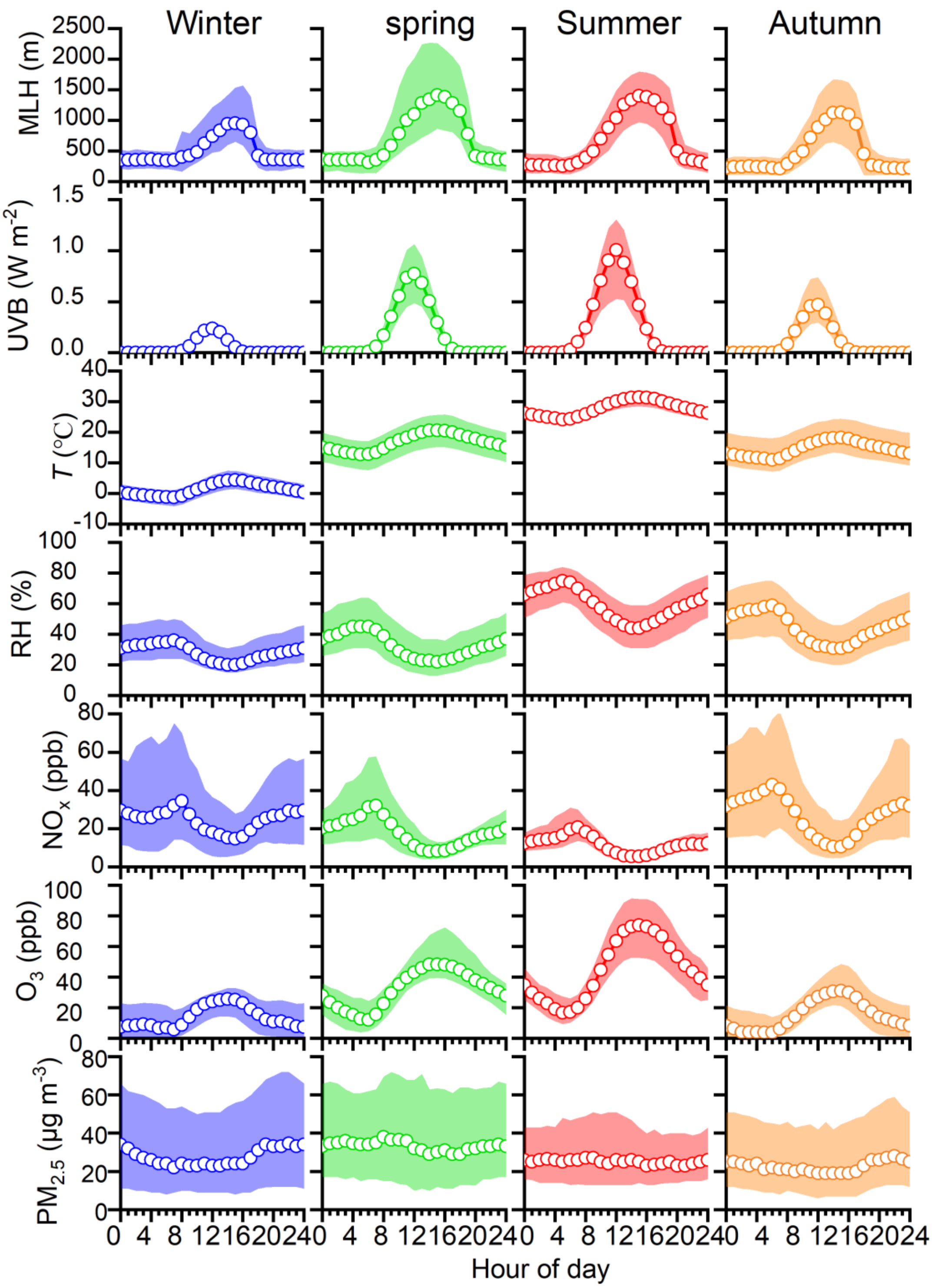

Figure S2. Diurnal variations of mixing layer height (MLH), solar radiation (UVB), temperature (T), relative humidity (RH), NO_x ($NO + NO_2$), O_3, and $PM_{2.5}$ concentrations in the four seasons.

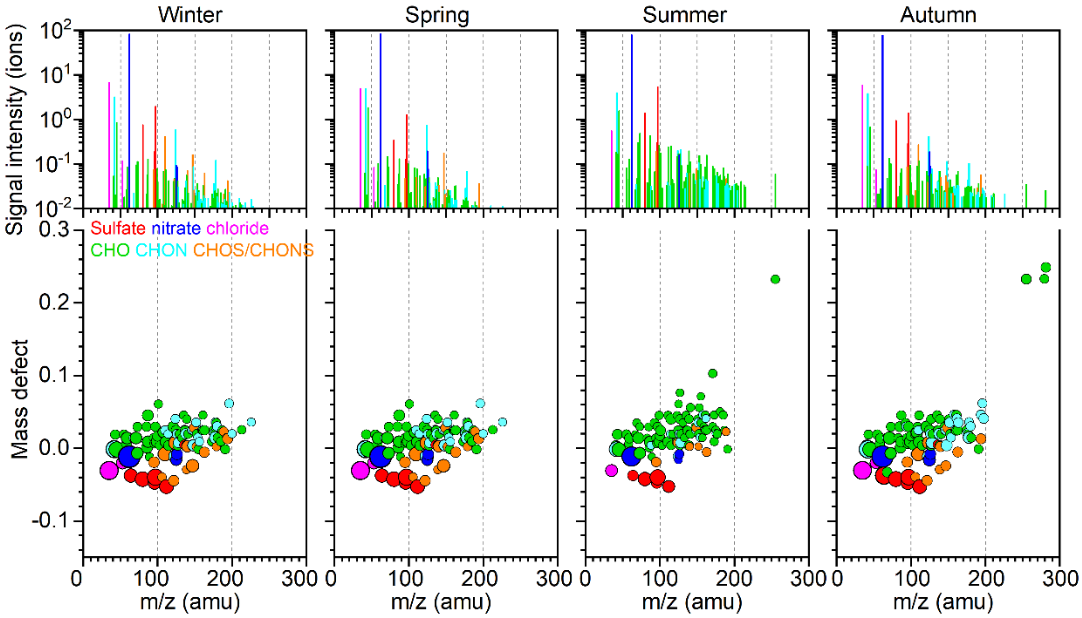

Figure S3. Details of the measured UFP composition over four seasons. (a) Mass spectra and (b) mass defect of compounds with the top 100 highest signals measured by the TDCIMS.

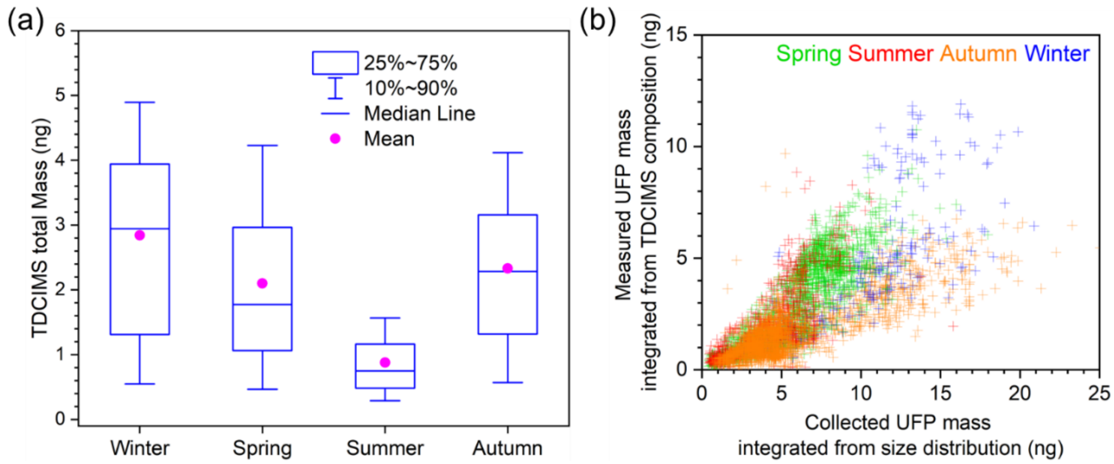

Figure S4. Seasonal variation of UFP mass (a) integrated from TDCIMS signals in negative ion mode; and (b) its comparison with collected UFP masses integrated from size distributions assuming spherical particles with a density of 1.4 g cm^{-3}.

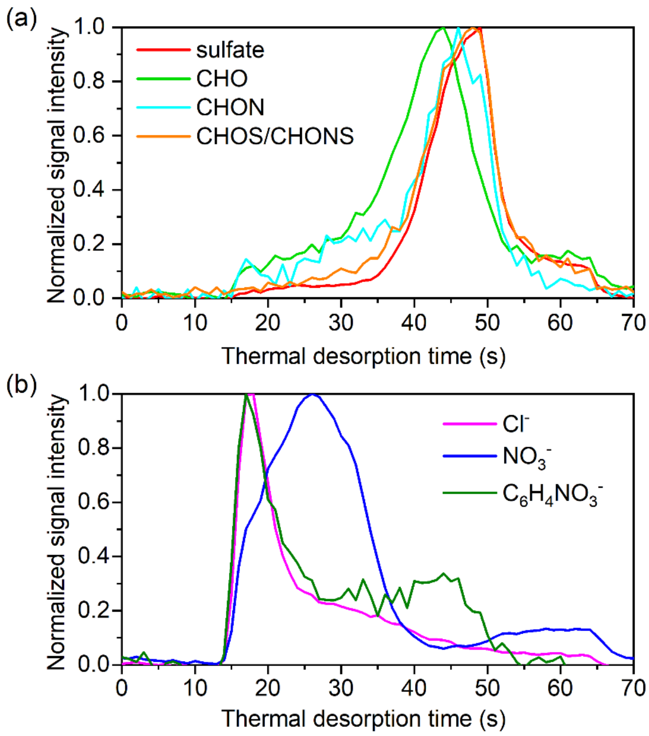

Figure S5. Averaged, normalized thermal desorption profiles of (a) the slowly desorbed compounds and (b) the quickly desorbed compounds. The signals are normalized to the corresponding highest signal of the thermal desorption curves.

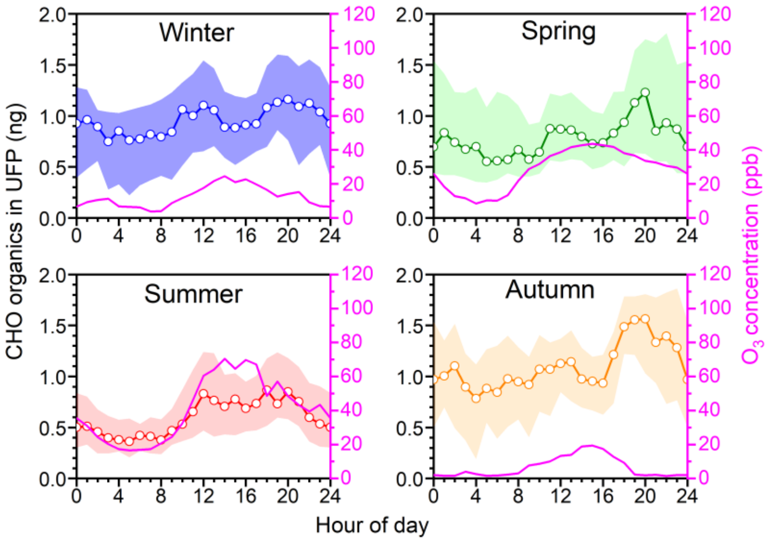

Figure S6. Diurnal variations of CHO organics and the corresponding O_3 variation over four seasons.

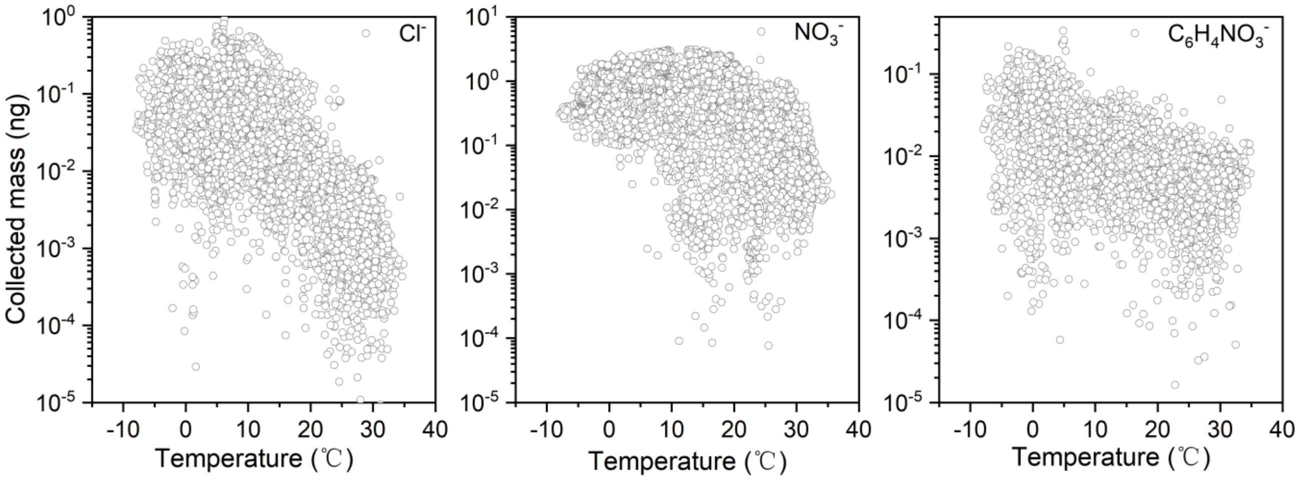

Figure S7. Negative temperature dependence of the quickly desorbed compounds (Cl^-, NO_3^-, and $C_6H_4NO_3^-$) in UFPs.

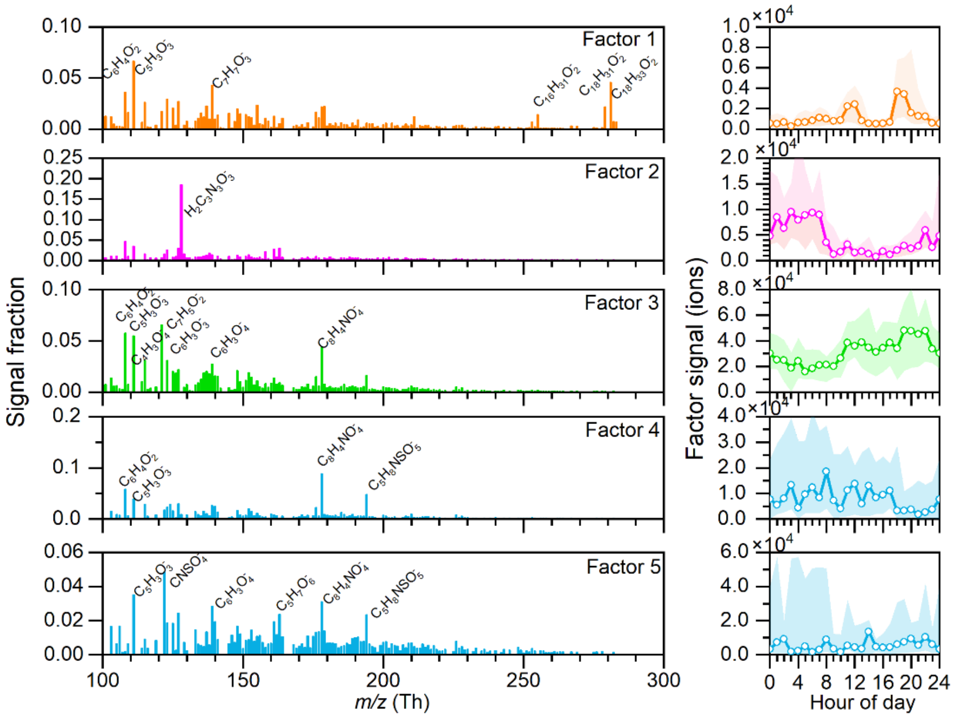

Figure S8. The PMF results for spring.

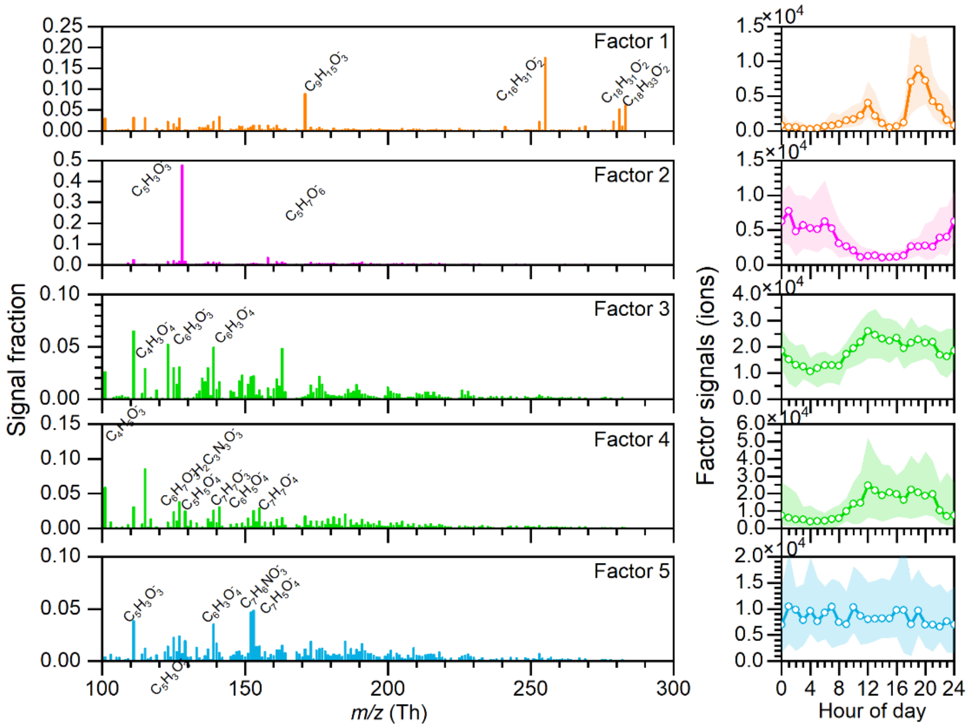

Figure S9. PMF results for summer.

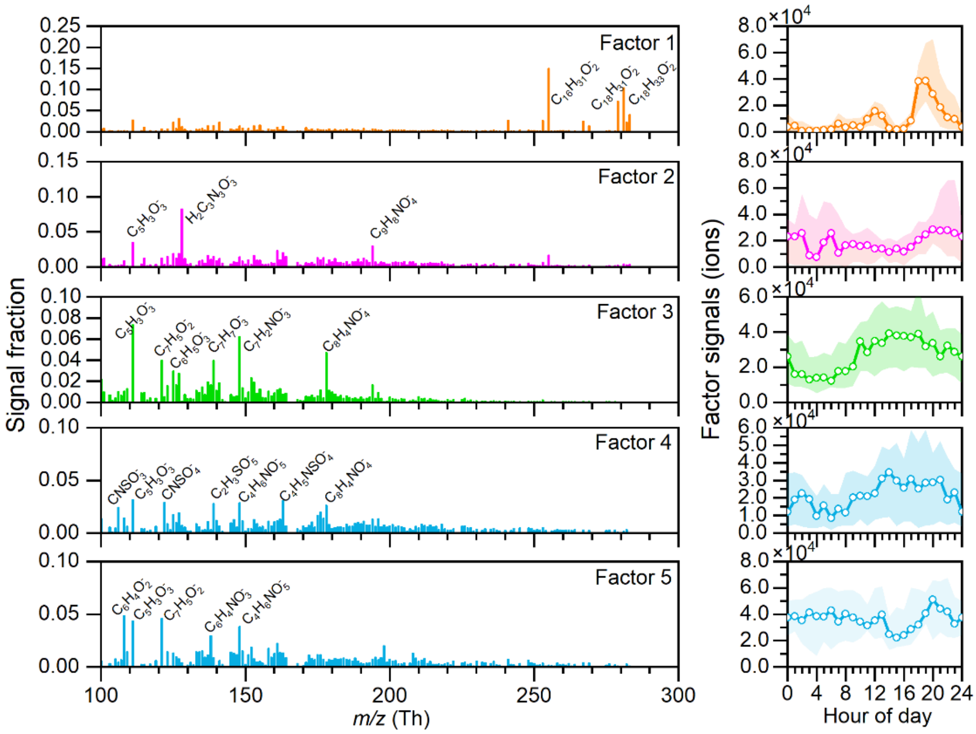

Figure S10. PMF results for autumn.

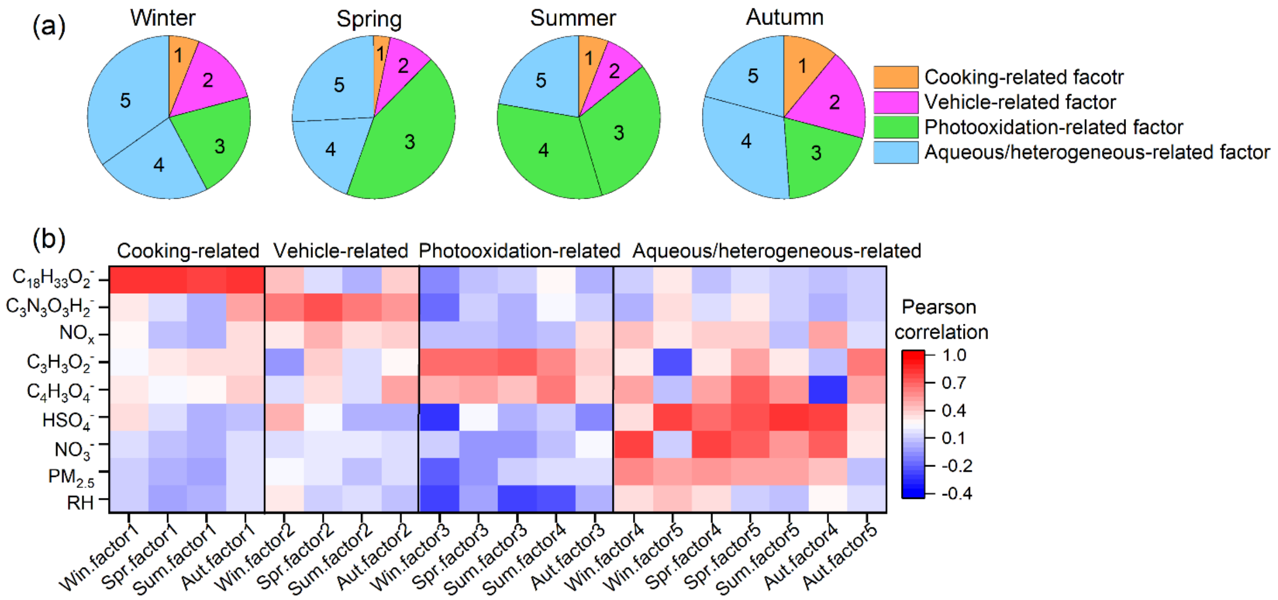

Figure S11. Summary of PMF factors during the four seasons. (a) PMF factor contribution for each season; (b) correlation of 5 factors with the measured key species, trace gas, and $PM_{2.5}$ for each season.

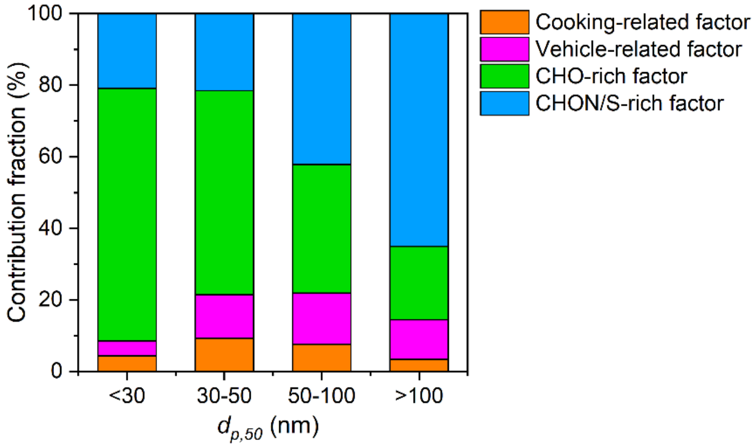

Figure S12. Contribution of different factors as a function of particle size. $d_{p,50}$ corresponds to 50% volume mean diameter of particles collected on the TDCIMS filament.

Table S1. Field measurement data summary.

Measurement targets	Instrumentation	Measuring periods	Notes
UFP composition	TDCIMS (bulk collection mode)	2021.1.18-2.14	Winter (24)
		2021.3.16-4.30	Spring (45)
		2021.7.11-8.27	Summer (47)
		2019.10.28-11.30	Autumn (33)
1 nm-10 μm particle size distribution	PSD & DEG-SMPS	2019.10.28-2021.8.27 Covering all of the above periods	Covering all of the above periods
Temperature, Solar radiation, Relative humidity	Weather station (AWS310, Vaisala)	2019.10.28-2021.8.27 Covering all of the above periods	Covering all of the above periods
NO_x, O_3	Thermo Fisher analyzer	2019.10.28-2021.8.27 Covering all of the above periods	Covering all of the above periods
Mixing layer height (MLH)	Ceilometer (CL51, Vaisala)	2019.10.28-2021.8.27 Covering all of the above periods	Covering all of the above periods